

A microfocus x-ray source based on a nonmetal liquid-jet anode

T. Tuohimaa,^{1,a)} J. Ewald,¹ M. Schlie,¹ J. M. Fernández-Varea,² H. M. Hertz,¹ and U. Vogt¹

¹*Biomedical and X-ray Physics, Department of Applied Physics, KTH Royal Institute of Technology/Albanova, SE-10691 Stockholm, Sweden*

²*Facultat de Física (ECM), Universitat de Barcelona, Diagonal 647, ES-08028 Barcelona, Spain*

(Received 18 March 2008; accepted 20 May 2008; published online 13 June 2008)

We demonstrate stable operation of a nonmetallic anode in an electron-impact x-ray source. A high-brightness electron beam is focused on a ~ 70 m/s speed, ~ 10 μm diameter methanol jet producing stable x-ray emission with peak spectral brightness at $\sim 5.4 \times 10^5$ photons/(s \times μm^2 \times sr \times 0.1% BW). The jet is fully evaporated in the interaction point. The shape of a simulated spectrum using Monte Carlo methods shows good agreement with experimental data, and the theoretical brightness values give an upper limit for the achievable x-ray emission from jets with very high velocities. Using this anode concept, all compounds and elements found in liquid form are potentially usable for x-ray generation. © 2008 American Institute of Physics. [DOI: 10.1063/1.2942379]

Microfocus electron-impact x-ray sources are gaining importance for a number of applications such as nondestructive testing, microtomography, phase contrast imaging, hard-x-ray microscopy, and x-ray diffraction.¹⁻⁵ Recently, microfocus electron-impact sources based on liquid-metal-jet anodes have demonstrated superior performance compared to conventional microfocus sources.⁶ To date, predominantly high-Z metal-jet anodes with a low melting point have been employed, thus limiting the range of characteristic line radiation available. In the present paper, we extend this class of jet-based sources by demonstrating stable operation of a nonmetal-jet anode at useful power levels. In addition, the performance limit of this class of anodes is investigated by simulating the x-ray emission with Monte Carlo techniques.

Conventional microfocus x-ray sources are limited in performance by the thermal properties of the anode⁷ with typical maximum e-beam power loads being in the range of 0.4–0.8 W per electron-beam diameter in micrometers [full width at half maximum (FWHM) of Gaussian beam]. In order to increase the x-ray brightness, liquid-metal-jet anodes have been proposed.⁸ They are attractive due to their higher thermal load capacity, regenerative nature, and the higher brightness achieved.⁹ E-beam loading capacities of >8 W/ μm have been demonstrated in continuous operation, more than an order of magnitude higher than what is achievable with conventional electron-impact technology.^{6,10}

Extending the jet anode concept to nonmetallic liquids would greatly increase the number of possible target elements giving access to numerous characteristic x-ray fluorescence lines. In an early low-power experiment directed toward soft-x-ray fluorescence emission, instabilities between a water jet and an e-beam at 10 keV occurred at powers above 0.6 W.¹¹ In the present paper, we show stable operation of a fully evaporated nonmetal (methanol) jet with significant hard x-ray emission. Methanol was chosen due to its high vapor pressure and low-conductivity properties, making it a good anode candidate for evaluating the limiting properties of low-Z, nonmetallic anode materials. Furthermore,

methanol has the additional advantage of generating vapor emission products that can be pumped away from the source area. This might be a problem for metal-jet anodes, where metal vapor is potentially deposited on all exposed surfaces, making a debris mitigation system necessary at high-power operation.^{12,13}

The experimental results are compared with Monte Carlo simulations using the PENELOPE code.¹⁴ By adapting the simulations to the cylindrical geometry of the jet, the theoretical limits for the x-ray emission from this class of anodes may be investigated.

The x-ray source with its nozzle arrangement for producing the methanol jet anode was situated in a vacuum chamber pumped with a 500 l/s turbo drag pump down to a base pressure of $\sim 10^{-7}$ mbar. By applying up to 40 bars of nitrogen backing pressure a stable ~ 70 m/s, ~ 10 μm diameter liquid-methanol jet was injected into the vacuum chamber via a tapered glass nozzle. The e-gun was based on a custom-made 50 μm diameter LaB₆ cathode¹⁵ with energies ranging from 10 to 50 keV and a maximum power of ~ 75 W. The beam was focused by a magnetic lens onto the methanol jet resulting in a high-brightness x-ray spot. The gun was optimized for operation at 50 keV and the Gaussian e-beam diameter (FWHM) at the focus was estimated to be 4–5 μm at 60 W and 50 keV from simulation results.¹⁶ Thus, the electron gun operated at 60 W and 50 keV could ideally achieve >12 W/ μm e-beam power loading, corresponding to approximately 2 MW/mm² e-beam power density at the target, more than enough to melt and permanently damage any conventional anode.

Differential pumping of the gun with a separate 250 l/s turbo drag pump kept the base pressure in the gun at $\sim 10^{-8}$ mbar when the jet was not running. The gun and jet chamber were separated by a 2.5 mm diameter aperture in the gun and a 6 mm aperture in the magnetic lens. Due to the high vapor pressure of methanol and the heating of beam, the pressures in the gun and jet chamber rose to $\sim 10^{-5}$ and $\sim 10^{-2}$ mbar, respectively. This was still good enough to get adequate transmission of the electron beam and the x rays produced in the interaction with the methanol jet. The complete system was carefully grounded to avoid charging phe-

^{a)}Electronic mail: tomi.tuohimaa@biox.kth.se.

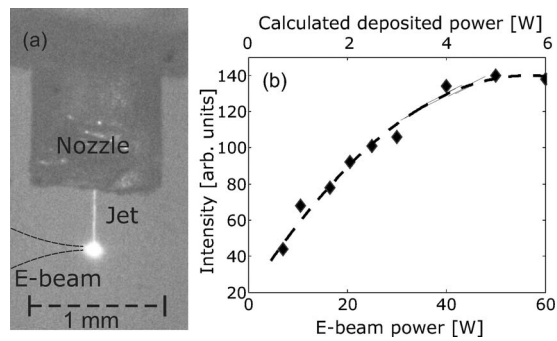


FIG. 1. (a) Microscope image of a ~ 70 m/s speed methanol jet interacting with a 50 keV, 70 W electron beam. (b) Integrated CCD intensity as a function of electron beam power. The dashed curve is fitted to the experimental data.

nomina and subsequent electron beam instabilities. An x-ray charge-coupled device (CCD) detector (Photonic Science VHR) was used for imaging in a projection geometry and a CdZnTe diode (Ref. 17) was employed for spectral flux measurements. The instruments operated at 45° and 90° , respectively, relative to the e-beam direction, thus enabling simultaneous recording of the spectrum and source size. The x-ray source size, needed for the absolute brightness calibration of the spectra, was determined via modulation measurements using a custom-made resolution object based on a $50\ \mu\text{m}$ thick silicon substrate with $10\ \mu\text{m}$ high gold structures.¹⁸ Lines down to $3\ \mu\text{m}$ half-period, corresponding to ~ 160 LP/mm² were available on the resolution target. The experimentally measured modulation could then be used to calculate the source size by comparing to simulated modulation curves using an adaptation of the code described in Ref. 6.

The general-purpose Monte Carlo code system PENELOPE was used for simulation of x-ray spectra.¹⁹ PENELOPE is applicable to all materials and covers the energy range from 50 eV up to 1 GeV. The code implements databases with reliable interaction cross sections and relaxation data for the elements. In particular, bremsstrahlung cross sections are taken from Seltzer and Berger's synthetic tables. The simulations assumed a $9\ \mu\text{m}$ diameter cylinder consisting of oxygen, carbon, and hydrogen atoms with fractions by weight corresponding to methanol. Jets injected into vacuum cool down by evaporative cooling and thus a density of $8.5\ \text{g/cm}^3$ was set for the cylinder, corresponding to methanol at 230 K and 1 bar. The e-beam focus hitting the cylinder was implemented as a Gaussian spatial distribution, with the impinging electron energies ranging from 20 to 50 keV.

All measurements with the methanol-jet anode were performed with electron beam powers at 5–70 W, substantially higher than previously recorded. The experimental results presented below are averages over many experiments, with special emphasis on the stability of the source at high deposited power levels, which is important for imaging applications. Figure 1(a) shows a microscope image of the interaction between the jet and a 50 keV e-beam at 70 W of power. The jet was totally evaporated at the e-beam focus and no signs of evaporation or charging-related source instabilities were observed. Monte Carlo calculations using PENELOPE indicate that $\sim 10\%$ of the e-beam power is absorbed at 50 keV. Figure 1(b) displays the recorded integrated x-ray intensity on the CCD as a function of e-beam power. The measured CCD signal shows saturation of the x-ray flux at

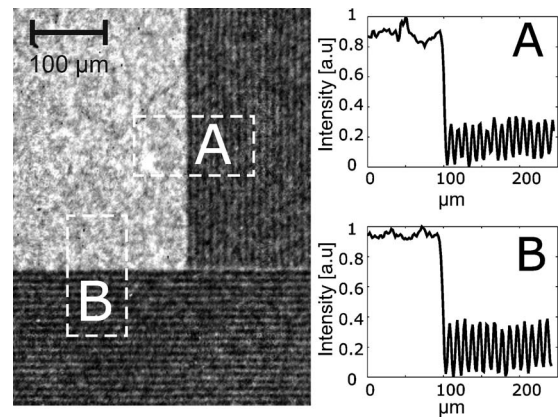


FIG. 2. (Left) CCD image of $5\ \mu\text{m}$ wide gold lines ($T=90$ s). (Right) Intensity profiles taken in the dashed areas in the image show good modulation of the vertical and horizontal lines.

high deposited power levels in good correspondence with the power (~ 6 W) required to totally evaporate the methanol jet. Figure 2 further illustrates the stability of the source within a typical exposure time (90 s) using an x-ray projection image of the resolution test target. The modulation of the $5\ \mu\text{m}$ wide gold lines (100 LP/mm) is good in both the vertical (A) and horizontal (B) directions, indicating a spatially stable x-ray source during the exposure.

The measured average x-ray source size was $44 \pm 21\ \mu\text{m}^2$ (1σ) with variations depending on the electron beam power, acceleration voltage, and the ability to center and focus the e-beam onto the jet. The minimum source size measured was $\sim 16\ \mu\text{m}^2$ at 40 W of e-beam power using a 50 keV beam, leading to an e-beam power density of $\sim 1.2\ \text{MW/mm}^2$, the highest power density ever recorded with the electron gun.

We observed a tendency to broadening of the x-ray spot at high deposited power (i.e., close to the total evaporation of the jet), especially at lower electron beam energies. This broadening is partially caused by the reduced focusing ability of the electron gun, but it is potentially also due to the increased electron-gas interaction and reduced jet density induced by the increased methanol vapor emission from the interaction area. Electron beam welding machines, utilizing similar power densities, uses this phenomenon to achieve deep penetration welding joints (>100 mm), although with stationary targets.²⁰

Spectra were measured for e-beam energies ranging from 20 to 50 keV, all at a constant e-beam current of 0.8 mA. Figure 3 shows a calibrated bremsstrahlung spectrum, recorded with a 50 keV, 40 W (~ 4 W deposited) electron beam with a peak spectral brightness of $\sim 5.4 \times 10^5$ photons/(s $\times\ \mu\text{m}^2 \times\ \text{sr} \times 0.1\% \text{ BW}$) at 10 keV. Although more power could be absorbed in the jet for low keV e beams and the measured x-ray flux increased, the e-beam focus got larger resulting in x-ray spot growth and hence slightly lower values for the spectral brightness at lower e-beam energies (20–40 keV). The average spectral brightness was $(3.6 \pm 1.3) \times 10^5$ photons/(s $\times\ \mu\text{m}^2 \times\ \text{sr} \times 0.1\% \text{ BW}$) for the investigated acceleration voltages in the range of 20 to 50 keV. Characteristic line emission was not visible in the 10–50 keV energy interval due to the low-Z composition of methanol.

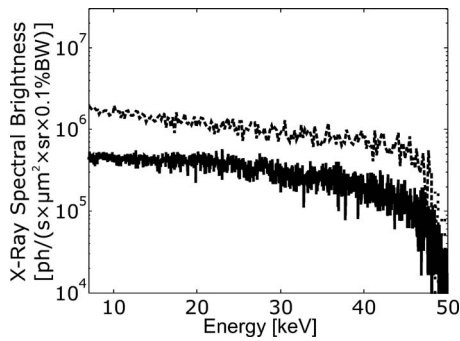


FIG. 3. Measured x-ray spectrum from the methanol-jet anode using a 50 keV, 40 W e-beam. The calibrated spectrum has been compensated for absorption in the air and the beryllium windows along with corrections for spot size, exposure time, and detector efficiency. The dashed upper curve shows the spectrum simulated with PENELOPE.

The Monte Carlo simulated spectrum, plotted with a dashed line in Fig. 3, has a spectral brightness of $\sim 1.6 \times 10^6$ photons/(s $\times \mu\text{m}^2 \times \text{sr} \times 0.1\% \text{ BW}$) at 10 keV. The brightness calculations for the simulated spectra were made using experimentally measured source sizes. The shape of the simulated spectrum is in good agreement with the experimental data, although the overall brightness is a factor of ~ 2 – 3 higher. This is thought to be due to the modeling of the jet as a nonmoving cylinder neglecting all thermodynamic phenomena such as jet boiling and subsequent density gradients that reduce x-ray production. Therefore the simulations give an upper limit for the x-ray brightness set by the input parameters and are valuable for understanding the ultimate performance of jet-based anodes with very high velocities.

To conclude, we have demonstrated stable x-ray operation of a nonmetallic liquid-jet anode at power levels sufficient to completely evaporate the jet in the e-beam focus. The maximum x-ray performance was found to be limited by the total evaporation of the jet material which occurred at ~ 6 W of absorbed e-beam power for the fastest jet used in the experiment. Larger and/or faster jets would overcome the present limit because of their inherently higher heat load capacities. We have previously shown that liquid jets can in principle be operated in a stable manner at much higher speeds in a vacuum environment.²¹ If the technological difficulties of increasing the jet speed could be overcome, the liquid-jet-anode concept would be an interesting alternative to existing compact x-ray sources, both for the hard and soft x-ray ranges. As an example, a water jet anode could be used

to emit *K*-shell x-ray radiation at 525 eV, making it a potential alternative to existing laser plasma²² or gas discharge sources.²³ To achieve this goal, further experimental work is necessary to investigate the long term stability and power scaling of such systems, in particular the lifetime of electron gun cathodes exposed to elevated gas loads.

The authors gratefully acknowledge the financial support of the Swedish Foundation for Strategic Research and the Swedish Research Council.

¹See, e.g., MicroXCT, nanoXCT (www.xradia.com).

²S. W. Wilkins, T. E. Gureyev, D. Gao, A. Pogany, and A. W. Stevenson, *Nature (London)* **384**, 335 (1996).

³V. E. Coslett and W. C. Nixon, *Nature (London)* **168**, 24, (1951).

⁴M. Wolkenhauer, G. G. Bumbu, Y. Cheng, S. V. Roth, and J. S. Gutmann, *Appl. Phys. Lett.* **89**, 054101 (2006).

⁵P. A. Lynch, A. W. Stevenson, D. Liang, D. Parry, and S. Wilkins, *Rev. Sci. Instrum.* **78**, 023904 (2007).

⁶T. Tuohimaa, M. Otendal, and H. M. Hertz, *Appl. Phys. Lett.* **91**, 074104 (2007).

⁷D. E. Grider, A. Wright, and P. K. Ausburn, *J. Phys. D: Appl. Phys.* **19**, 2281 (1986).

⁸O. Hemberg, M. Otendal, and H. M. Hertz, *Appl. Phys. Lett.* **83**, 1483 (2003).

⁹O. Hemberg, M. Otendal, and H. M. Hertz, *Opt. Eng. (Bellingham)* **43**, 1682 (2004).

¹⁰M. Otendal, T. Tuohimaa, and H. M. Hertz, *Rev. Sci. Instrum.* **79**, 016102 (2008).

¹¹B. Buijsse, *Proc. SPIE* **4502**, 74 (2001).

¹²M. Otendal, T. Tuohimaa, and H. M. Hertz, *J. Appl. Phys.* **101**, 026102 (2007).

¹³J. Pankert, R. Apetz, K. Bergmann, G. Derra, M. Janssen, J. Jonkers, J. Klein, T. Krücken, A. List, M. Loeken, C. Metzmacher, W. Neff, S. Probst, R. Prümmer, O. Rosier, S. Seiwert, G. Siemons, D. Vaudrevange, D. Wagemann, A. Weber, P. Zink, and O. Zitzen, *Proc. SPIE* **5751**, 260 (2005).

¹⁴F. Salvat, J. M. Fernández-Varea, and J. Sempau, *PENELOPE-2006 A Code System for Monte Carlo Simulation of Electron and Photon Transport* (OECD, Nuclear Energy Agency, Issy-les-Moulineaux, France, 2006).

¹⁵See, e.g. (<http://www.a-p-tech.com/grcathodes.htm>).

¹⁶LORENTZ2EM v.6.2 (www.integratedsoft.com).

¹⁷XR-100T-CZT (www.amptek.com).

¹⁸J. Reinspach, "Contact Lithography for X-ray Optics," M.S. Thesis, Royal Institute of Technology, 2007.

¹⁹X. Llovet, J. M. Fernández-Varea, J. Sempau, and F. Salvat, *Surf. Interface Anal.* **37**, 1054 (2005).

²⁰H. Schwarz, *J. Appl. Phys.* **35**, 2020 (1964).

²¹M. Otendal, O. Hemberg, T. T. Tuohimaa, and H. M. Hertz, *Exp. Fluids* **39**, 799 (2005).

²²P. A. C. Jansson, U. Vogt, and H. M. Hertz, *Rev. Sci. Instrum.* **76**, 043503 (2005).

²³R. Lebert, K. Bergmann, G. Schriever, and W. Neff, *Microelectron. Eng.* **46**, 465 (1999).